

# Stability and Nuclear Dynamics of the Bicoid Morphogen Gradient

Thomas Gregor,<sup>1,2,3,4,\*</sup> Eric F. Wieschaus,<sup>3,4</sup> Alistair P. McGregor,<sup>5</sup> William Bialek,<sup>1,2</sup> and David W. Tank<sup>1,2,3</sup>

<sup>1</sup>Lewis-Sigler Institute for Integrative Genomics

<sup>2</sup>Joseph Henry Laboratories of Physics

<sup>3</sup>Department of Molecular Biology

<sup>4</sup>Howard Hughes Medical Institute

<sup>5</sup>Department of Ecology and Evolutionary Biology

Princeton University, Princeton, New Jersey 08544, USA

\*Correspondence: tg2@princeton.edu

DOI 10.1016/j.cell.2007.05.026

## SUMMARY

Patterning in multicellular organisms results from spatial gradients in morphogen concentration, but the dynamics of these gradients remain largely unexplored. We characterize, through in vivo optical imaging, the development and stability of the Bicoid morphogen gradient in *Drosophila* embryos that express a Bicoid-eGFP fusion protein. The gradient is established rapidly (~1 hr after fertilization), with nuclear Bicoid concentration rising and falling during mitosis. Interphase levels result from a rapid equilibrium between Bicoid uptake and removal. Initial interphase concentration in nuclei in successive cycles is constant ( $\pm 10\%$ ), demonstrating a form of gradient stability, but it subsequently decays by approximately 30%. Both direct photobleaching measurements and indirect estimates of Bicoid-eGFP diffusion constants ( $D \leq 1 \mu\text{m}^2/\text{s}$ ) provide a consistent picture of Bicoid transport on short (~min) time scales but challenge traditional models of long-range gradient formation. A new model is presented emphasizing the possible role of nuclear dynamics in shaping and scaling the gradient.

## INTRODUCTION

The most widely accepted conceptual framework for pattern formation in developing multicellular organisms is the morphogen gradient: a spatially varying concentration of a transcription factor or extracellular signaling molecule across a field of developing cells in which cells acquire information about their spatial location from local measurements of morphogen concentration (Wolpert, 1969). Although molecular studies have identified candidate

morphogens and demonstrated that cells can respond differently to different concentrations of these molecules (Lawrence, 1992; Driever and Nüsslein-Volhard, 1988b; Zecca et al., 1995; Ariizumi and Asashima, 1995), the mechanisms that produce the gradients and read out positional information are not understood.

One of the best studied morphogen gradients is the Bicoid (Bcd) gradient in early *Drosophila melanogaster* embryos (Driever and Nüsslein-Volhard, 1988a; Struhl et al., 1989; Ephrussi and St Johnston, 2004). Bcd is a maternal anterior determinant in the developing embryo that controls anterior-posterior (AP) patterning. Its mRNA is deposited during oogenesis at the anterior pole of the egg and is translated soon after fertilization. Antibody staining in fixed embryos demonstrates that Bcd concentration decays approximately exponentially with distance from the anterior pole. The exponential shape is consistent with the gradient being formed by a balance of localized synthesis, diffusion, and spatially uniform degradation (Crick, 1970; Lacalli and Harrison, 1991), which we will refer to as the SDD model. Important unmeasured parameters in the SDD model are the diffusion coefficient ( $D$ ) of Bcd and its lifetime ( $\tau$ ) in the cytoplasm. In general, the model remains untested, and alternatives, such as active transport, have not been ruled out.

The dynamic properties of the Bcd gradient have not previously been characterized. For example, it is unknown how quickly the gradient is established and whether or not its amplitude and shape evolve or fluctuate with time. Characterizing these dynamics is important both for defining the plausibility of mechanisms implied by the SDD model and for defining what positional information actually is available for morphogen readout. In the simplest SDD model implementation, the concentration profile of Bcd reaches a steady state, and this requires some minimum time that depends on the Bcd diffusion coefficient. Is the actual development time of the Bcd gradient consistent with its diffusion coefficient? Similarly, the mechanism of gradient readout might necessarily be more complex than a single time point measurement of concentration if the gradient is found to change shape or fluctuate significantly.

Our understanding of the development and stability of the Bcd gradient has been limited by the use of fixed tissue and antibody staining techniques that provide only static snapshots of the morphogen distribution. In addition, the analysis is complicated by the fact that the gradient arises during a stage when the embryo is undergoing rapid syncytial nuclear mitoses. As expected for a transcription factor, Bcd protein localizes to nuclei during interphase, but during mitosis nuclear envelopes break down, and it is unknown if the gradient is affected. Are events inside the nucleus responding passively to a gradient established in the surrounding cytoplasm, or do intranuclear processes help to shape the gradient itself? Along these lines, it recently has been suggested that Bcd degradation in nuclei contributes to the mechanism for scaling across embryos of different sizes (Gregor et al., 2005).

Here we address these issues with a dynamic measurement of the Bcd gradient in single embryos. Fly transformants that encode a fusion gene of *bcd* and the coding region of the enhanced green fluorescent protein (eGFP) were generated. By observing these transformants with time-lapse two-photon fluorescence microscopy and photobleaching methods, the dynamics of the Bcd gradient were measured and perturbed during the first three hours of embryonic development. We show that the gradient is formed within the first hour after egg fertilization and that it then is stably maintained during blastodermal stages. After each mitotic division, the concentration of Bcd in nuclei at a given position along the AP axis of the egg reaches the same value it had in the previous nuclear cycle with a precision of 10%, despite changes in nuclear size and density. The nuclear and cytoplasmic concentrations are shown to be in a dynamic equilibrium on the  $\sim 1$  min time scale. Direct and indirect measurements of the Bcd diffusion constant are all consistent with  $D \sim 0.3 \mu\text{m}^2/\text{s}$ , which is much smaller than expected and raises problems for understanding how it is possible for the gradient to be established so rapidly. Finally, we propose a variant of the SDD model, involving nuclear degradation, that captures the Bcd dynamics revealed in our measurements and emphasizes a role for those dynamics in solving the scaling problem.

## RESULTS

### Bcd-GFP Construct: Initial Characterization

To visualize the spatiotemporal dynamics of Bcd concentration we made transgenic *Drosophila* embryos in which endogenous Bcd was replaced with a fluorescent eGFP-Bcd fusion protein (called Bcd-GFP hereafter). Flies were generated utilizing a transcript coding for eGFP (Tsien, 1998) fused to the N terminus of Bcd. As in previous work with a GFP (rather than eGFP) fusion protein (Hazelrigg et al., 1998), the construct contained endogenous *bcd* 5' and 3' UTRs, which are known to mediate anterior localization and translation of *bcd* mRNA.

Embryos expressing Bcd-GFP demonstrated an intricate spatial and temporal pattern of concentration

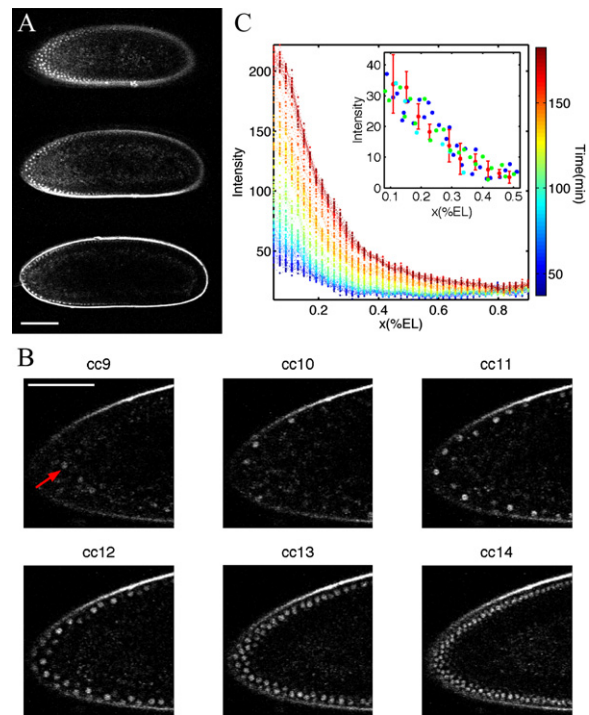


**Figure 1. Time-Lapse Movie of a *Drosophila* Embryo Expressing Bcd-GFP Using Two-Photon Microscopy**

(A) Typical image stack during nuclear cycle 12 of three focal planes at 30  $\mu\text{m}$  (top panel), 60  $\mu\text{m}$  (middle panel), and 90  $\mu\text{m}$  (bottom panel) below the top surface of the embryo. (Scale bar is 100  $\mu\text{m}$ .)

(B) Six snapshots of a time-lapse movie of the anterior third of the mid-sagittal plane of a *Drosophila* embryo expressing Bcd-GFP. Each snapshot corresponds to a time point during interphases 9 to 14. Red arrow points to individual nucleus during interphase 9 when nuclei are deeper inside the egg. (Scale bar is 60  $\mu\text{m}$ .)

(C) Bcd-GFP fluorescence profiles are extracted from two-photon time-lapse movies and projected on the egg's AP axis by sliding (in software) an averaging box of  $10 \times 10 \mu\text{m}^2$  size along the edge of the egg focused at the midsagittal plane. Time is represented by color code. Time zero corresponds to oviposition. Imaging started  $20 \pm 15$  min after oviposition.

Inset shows nuclear Bcd gradients in nuclear cycles 11 (cyan), 12 (red), 13 (green), and 14 (blue) projected on the AP axis in the anterior half of the embryo (red error bars for nuclear cycle 12 are over five consecutive time points).

dynamics that was captured by time-lapse two-photon excitation laser scanning microscopy (Denk et al., 1990; Svoboda et al., 1997). A typical image stack of three focal planes from a Bcd-GFP embryo during nuclear cycle 12 is shown in Figure 1A. The fluorescence consisted of two components: bright nuclei and dispersed cytoplasmic fluorescence of lower intensity. The bright nuclei are consistent with previous antibody stainings of Bcd and the fact that Bcd is a transcription factor that should, at some point, be targeted to nuclei. A gradient in fluorescence intensity from anterior to posterior is observed in both the nuclear and cytoplasmic components, which is also consistent with previous work (Driever and Nüsslein-Volhard, 1988a; Movie S1).

Fluorescence from Bcd-GFP was first detected in anterior surface nuclei during nuclear cycle 9, approximately 90 min after fertilization. As shown in Figure 1B, during each successive nuclear division 9–14, bright nuclei reappear during interphase in the cortical layer. Qualitatively, these images reveal that in any given perimeter region, the total amount of fluorescence increases with each division. However, the intensity within individual nuclei at a given spatial location appears, qualitatively, to be the same. To provide initial quantification of these effects, at each time point fluorescence was measured within a rectangular region (containing several nuclei and surrounding cytoplasm) that was slid along the embryo perimeter (Houchmandzadeh et al., 2002). As shown in Figure 1C, a fluorescence gradient that is approximately an exponential function of distance along the embryo can first be measured about one hour after fertilization. The overall intensity increases progressively with development time. In contrast, as shown in the inset to Figure 1C, the intensity measured in a very small box within individual nuclei maintains a fixed profile as a function of distance along the embryo. Both the shape of the spatial decay and the absolute concentration do not appear to change, within measurement error, as a function of nuclear cycle.

A series of control experiments was performed to test the biological relevance of these measurements from two different perspectives. First, we asked the question: Does Bcd-GFP functionally substitute for endogenous Bcd, and do flies expressing Bcd-GFP develop normally? Second, we asked: Does the GFP fluorescence quantitatively represent the distribution of Bcd-GFP, and how does this distribution compare to that of endogenous Bcd?

First, the P[*egfp-bcd*] transgene completely rescues the headless anterior defect normally observed in embryos from *bcd* mutant mothers; qualitatively, no developmental defects are observed throughout the entire life cycle. Quantitatively, the position along the AP axis of the cephalic furrow, a strong indicator of the total amount of active Bcd protein, was measured. In embryos with the Bcd-GFP construct in a *bcd* null mutant background, the furrow location at  $32.8 \pm 1.3\%$  egg length (mean and standard deviation [SD] over  $n = 10$  embryos) was identical to that of wild-type embryos ( $33.8 \pm 0.7\%$ ;  $n = 12$ ); these results are consistent with previous qualitative estimates of approximately 35% (Driever and Nüsslein-Volhard, 1988b). Thus, by both qualitative and quantitative criteria, fluorescent *egfp-bcd* behaves indistinguishably from wild-type *bcd* in the early embryo, indicating that its localization and translational regulation are conserved and that the protein is folded properly despite the attached eGFP epitope.

Second, to determine the faithfulness with which eGFP fluorescence reports both Bcd-GFP and endogenous Bcd concentration, fixed embryos were colabeled with fluorescent antibodies against Bcd and GFP, and the fluorescence intensities at locations around the perimeter were compared to each other and to endogenous GFP fluorescence. As summarized in the scatter plots in Figure 2, the

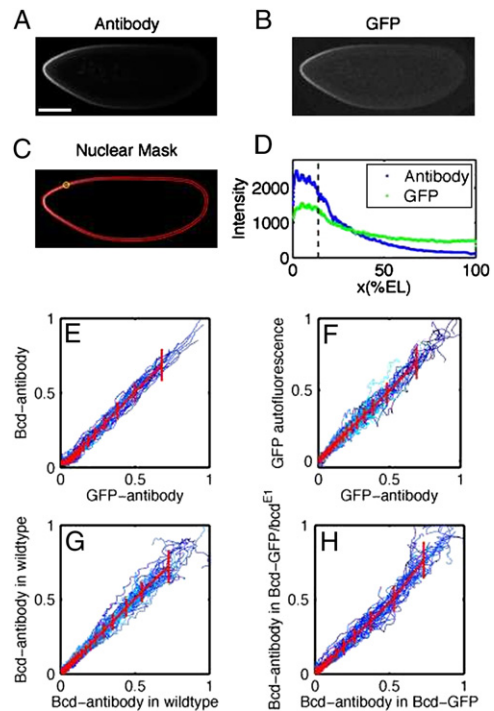


**Figure 2. Comparison of Bcd Profiles in *Drosophila* Embryos Expressing Bcd-GFP**

(Embryos were formaldehyde fixed during nuclear cycle 14 and imaged at the midsagittal plane via confocal microscopy.)

(A) Embryo stained with GFP antibodies. (Scale bar is 100  $\mu\text{m}$ .)

(B) GFP autofluorescence for the same embryo as in (A).

(C) Nuclear layer obtained via image analysis software used to extract gradients from (A) and (B) by sliding a circular averaging area (yellow circle) along the edge of the embryo images.

(D) Extracted raw gradients from (A) and (B) projected on embryo AP axis. Dashed line corresponds to location of yellow circle in (C) from cut sections of (A); mean and SD across embryos.

(E–H) Scatter plots of fluorescence intensities extracted from Bcd profiles for different embryos. All profiles were normalized by background subtraction and a scale factor (see Experimental Procedures). Both dorsal and ventral profiles are shown in each panel. Colors represent individual embryos, red lines correspond to the average profile scatter, and error bars are for equal amounts of data points. Deviations of the compared profiles from the diagonal indicate a difference in the shape of the profile. For more information see Supplemental Data.

intensity of one probe always is linearly related to the intensity of a different probe. These results demonstrate that, except for differences in background levels, the fluorescence intensity in each case is proportional to the protein concentration. Further implications of these studies, such as the linearity of antibody staining as a method of quantifying relative protein concentration, are discussed in Supplemental Data.

Together, these control experiments reveal that the biological and physical properties of the Bcd-GFP construct reproduce the properties of the endogenous *bcd* gene. Thus our time-lapse observations of dynamics in Bcd-GFP-expressing embryos with a *bcd* null mutant

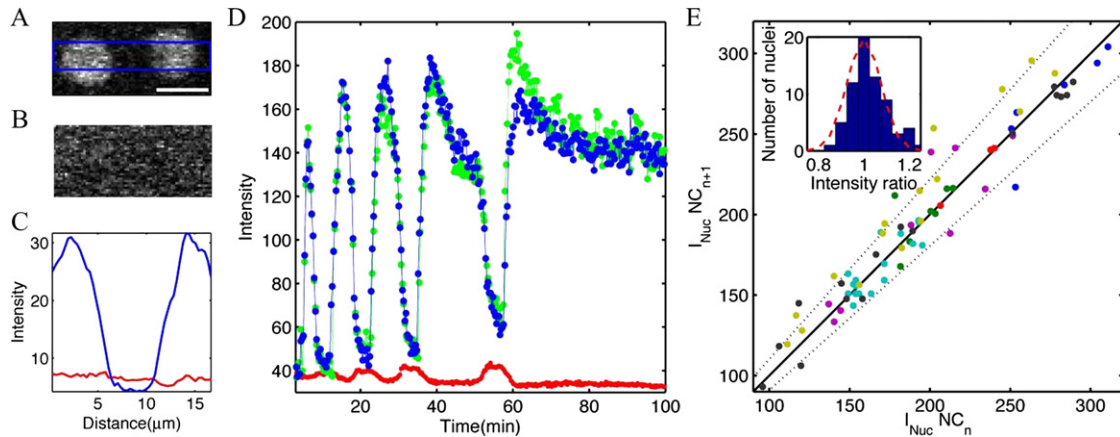


**Figure 3. Bcd Gradient Stability**

(A) Close-up of two adjacent nuclei expressing Bcd-GFP fluorescence during midinterphase 12. (Scale bar is 10  $\mu\text{m}$ .)

(B) Same field of view as in (A) during mitosis 13.

(C) Intensity profile of a mean horizontal cross-section through images in (A) and (B), with blue line indicating vertical average over blue rectangle in (A), and with red line indicating vertical average over entire image in (B).

(D) Typical nuclear and cytoplasmic development of Bcd-GFP concentration from nuclear cycles 10 to 14. Each data point corresponds to the concentration of a single nucleus at a given time point, computed as the mean intensity value over an area that corresponds to the smallest nuclear size encountered over the entire time course (384 pixels). Blue and green traces follow two individual nuclei (located at  $\sim 50 \mu\text{m}$  distance from the anterior pole of the embryo), and red curve corresponds to the average concentration in the interstitial space between the nuclei over a field of view of  $50 \times 50 \mu\text{m}$  (linear pixel dimension  $0.20 \mu\text{m}/\text{pixel}$ ). Time points are in 20 s intervals.

(E) Scatter plot of peak nuclear intensities  $I_{\text{Nuc}}$  averaged over 1–5 time points during nuclear cycle  $n$  versus nuclear cycle  $n + 1$ . Different colors represent different embryos ( $n = 7$ ). For each embryo one to eight nuclei were compared in nuclear cycles 10 to 14, resulting in a total of 77 data points. Black line with slope one corresponds to perfect intensity reproducibility across nuclear cycles. Dotted line corresponds to an accuracy of 10%. Inset bars indicate histogram of observed intensity ratios in bins of width 5%. Dashed line indicates results expected for Gaussian variations having the observed standard deviation of 7.9%.

background quantitatively represent wild-type behavior of the Bcd morphogen gradient.

### Constancy of Nuclear Bcd Concentration

The low magnification time-lapse movies in Figure 1 provide initial support for the idea that the gradient in intranuclear Bcd concentration along the embryo develops early and is approximately constant in amplitude and shape over time during nuclear cycles 9–14. This stability is, however, somewhat surprising, since several processes are occurring simultaneously that would be expected to produce local spatial and temporal variations in Bcd concentration: The number of nuclei doubles with each mitotic cycle, the size (diameter) of individual nuclei changes during interphase and between adjacent cycles, and Bcd concentrations must rise and fall as nuclear membranes form and dissolve. To further characterize and understand these expected changes in Bcd concentration and what kind of stability may exist at the local level, individual nuclei were tracked over time at higher magnification.

High-resolution time-lapse images were taken of nuclei in the anterior half of the embryo, with the field of view reduced to  $50 \times 50 \mu\text{m}^2$ . Figure 3A depicts two nuclei during interphase 12; the same field of view during mitosis 13 is shown in Figure 3B. The concentration profiles of a thin horizontal rectangle across the center of the nuclei in Figure 3A and the corresponding position in Figure 3B,

depicted in Figure 3C, clearly show that the cytoplasmic concentration increases during mitosis at the location between the two nuclei, as expected if Bcd-GFP is freed to diffuse into the cytoplasm as the nuclei enter mitosis.

To measure the complete time course of nuclear Bcd-GFP concentration from time-lapse movies during cycles 10–14, a fixed-size region of interest (ROI) within the nuclear membrane boundary of a single nucleus was determined during interphase. The average intensity within this ROI was determined for a sequence of images starting with the cytoplasm before nuclear membrane formation, through interphase, and continuing in the cytoplasm immediately following nuclear envelope breakdown. To continue the time course into the succeeding cycle, the ROI was switched to an area within the newly forming nucleus that was closest to the position of the first nucleus in order to maintain positional constancy along the AP axis of the egg. Figure 3D shows two time courses of nuclear concentration, determined by this procedure, from the same embryo.

These data demonstrate a stereotyped response in which peak intranuclear concentrations occur early in each syncytial nuclear cycle. They further reveal that these peaks are nearly constant between nuclear cycles 10 and 14. This is quantified by plotting, in Figure 3E, the concentration in one cycle against that in the preceding cycle. When monitoring three to four nuclei in each of seven

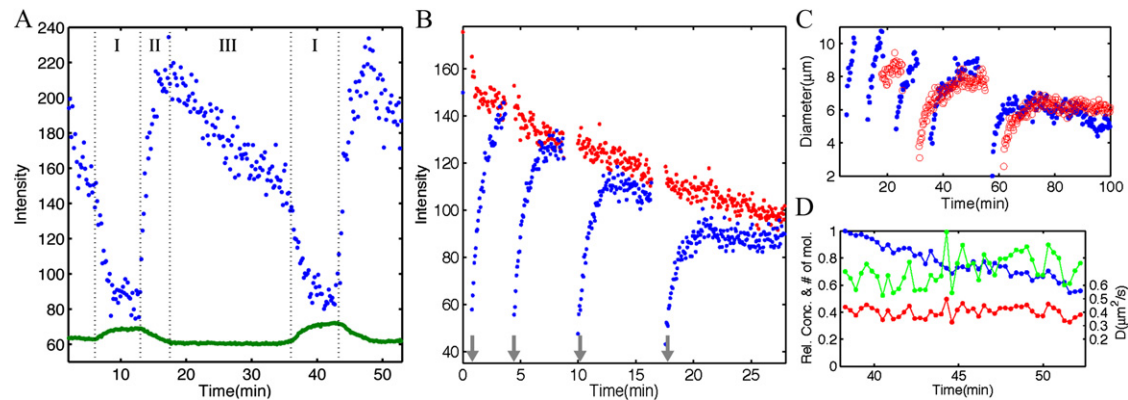


**Figure 4. Nuclear Bcd Concentration Dynamics**

(A) Typical nuclear (blue) and cytoplasmic (green) Bcd-GFP concentration development during nuclear cycle 13. Three intervals correspond to: (1) Nuclear envelope breakdown and diffusive nuclear Bcd-GFP release, (2) rapid refilling of newly formed nuclei after mitosis, and (3) interphase 13. (B) Fluorescence recovery after photobleaching of a single nucleus of a Bcd-GFP embryo during interval III of nuclear cycle 14. Blue curves are the recovery curves of a four times successively bleached nucleus, and red curve is the concentration in a neighboring unbleached nucleus. Bleach pulses (10–15 s long) are indicated by gray arrows. Data points are in 4 s intervals. The time constants  $\tau$  of exponential recovery fits are 60 s, 53s, 52s, and 50s, respectively, for the four bleaching traces. The linear decay of the red curve is due to the increasing nuclear diameter during interphase which leads to an effective decrease in the nuclear Bcd-GFP concentration (see text). (C) Development of nuclear diameter from nuclear cycle 10 to 14. Blue and red data points correspond to two different embryos (blue corresponds to the data set of Figure 3A). The nuclear diameters at the end of interphase (averaged over two embryos) in nuclear cycles 10 to 14 are 10.0  $\mu\text{m}$ , 10.5  $\mu\text{m}$ , 9.2  $\mu\text{m}$ , 8.2  $\mu\text{m}$ , and 6.5  $\mu\text{m}$ , respectively. (D) Relative intensity (blue), relative number of molecules (green), and ratio of number of molecules to influx (red) as a function of time during nuclear cycle 13. Blue curve corresponds to average nuclear intensity  $I(t)$  represented by the blue trace in Figure 3D during interphase 13. Green curve corresponds to the product of  $I(t)r_n^3(t)$ , where  $2r_n(t)$  is the nuclear diameter represented by the blue trace in (C). Red curve corresponds to the product  $I(t)r_n^2(t)$ . The right side of the vertical axis has been normalized to yield the cytoplasmic diffusion constant  $D = r_n^2 C_{in} / 3\tau C_{out}$ ; see text. To quantify the observation that  $I(t)r_n^2(t)$  is constant while  $I(t)r_n^3(t)$  is not, we looked for linear correlations between these quantities and time; for  $I(t)r_n^2(t)$  the correlation (0.50) is highly significant ( $p = 0.0013$ ), while for  $I(t)r_n^3(t)$  there is essentially no correlation (0.01,  $p = 0.93$ ); data sets for five embryos showed similar results.

different embryos, in most cases the peak is reproducible to better than 10% accuracy. More quantitatively, the ratio of fluorescence intensities from one cycle to the next has a mean of 1.02 and a standard deviation of just 7.9% ( $n = 77$ ). These results hold over a wide range of absolute concentrations, corresponding to positions from 5% to 35% of the distance from anterior to posterior pole.

Figure 3D also shows the cytoplasmic Bcd-GFP concentration across nuclear cycles 10–14. As for the nuclear concentration, a highly reproducible pattern between interphase and mitosis is observed with cytoplasmic concentration peaks during mitosis representing the equilibration of Bcd-GFP concentration after release from the nuclei, as shown in Figure 3C.

Our data show a surprising coexistence of highly dynamic behavior and precise constancy. Over the course of a single nuclear cycle, the concentration of Bcd varies systematically over a factor of four at the location corresponding to a single nucleus. When the next cycle starts, however, the nuclear Bcd concentration is restored to the same value with  $\sim 10\%$  accuracy. This reproducibility validates a dynamic version of the positional information hypothesis: From one nuclear cycle to the next, Bcd concentration provides information about the spatial location of the nucleus, and the mapping from position to con-

centration is invariant across cycles. This stability in the nuclear concentration gradient occurs despite the fact that the total concentration of Bcd in a local cortical region containing multiple nuclei is increasing with each cycle.

#### Nucleo-Cytoplasmic Bcd Concentration Equilibrium

Although peak Bcd concentrations are reproduced from one nuclear cycle to the next, closer inspection of the nuclear concentration time courses reveals a highly dynamic pattern, both in relative and in absolute terms. We identify three distinct behaviors of nuclear Bcd-GFP concentration during each mitotic cycle, marked as intervals I (nuclear envelope breakdown), II (refilling), and III (interphase) during nuclear cycle 13 in Figure 4A. Note that during interphase interval III, a concentration drop of approximately 30% is observed.

A fundamental question raised by our results is whether the high intranuclear concentration of Bcd results from simple trapping of Bcd or from a dynamic equilibrium of Bcd molecules exchanging between cytoplasm and the nuclei. To address this question, we bleached the fluorescence of Bcd-GFP in single nuclei during interphase. Nuclear fluorescence recovered, demonstrating that Bcd-GFP is being transported across the nuclear membrane.

A typical recovery trace of a single bleached nucleus in cycle 14 is shown in Figure 4B. If it is repetitively bleached during the slow interphase decay (interval III), the recovering concentration asymptotically approaches the intensity level of adjacent control nuclei. These data suggest that there is a dynamic equilibrium between transport into the nucleus and a loss, either via outward transport or intranuclear protein degradation.

To interpret the results of the photobleaching experiments more quantitatively, a simple model is considered in which molecules are transported into the nucleus at a rate proportional to the concentration outside in the cytoplasm ( $k_{in}C_{out}$ ) and leave the nucleus either from transport back into the cytoplasm (at rate  $k_{out}$ ) or by degradation (at rate  $k_{d-nuc}$ ). The dynamics for the number of molecules within a nucleus  $n(t)$  is given by

$$\frac{dn(t)}{dt} = k_{in}C_{out} - \frac{1}{\tau_n}n(t), \quad (1)$$

$$\frac{1}{\tau_n} = k_{out} + k_{d-nuc}, \quad (2)$$

where  $\tau_n$  is the effective lifetime of the molecule in the nucleus. If the cytoplasmic concentration is approximated as being constant during the measurement (consistent with experiment, see Figure 3D), then if the photobleaching pulse reduces the number of fluorescent molecules by an amount  $\Delta n_0$ , the model predicts an exponential recovery

$$n(t) = n_{\infty} - \Delta n_0 \exp(-t/\tau_n), \quad (3)$$

where  $n_{\infty} = k_{in}\tau_n C_{out}$  is the steady state number of molecules in the nucleus, and the observable fluorescence is proportional to the number of molecules  $n(t)$ . Notice that although recovery of fluorescence after photobleaching provides evidence for Bcd transport into the nucleus, the actual time constant for exponential recovery is related to the rate at which molecules leave the nucleus, either by export or degradation.

Following Equation 3, exponential functions were fit to 19 fluorescence recovery curves from four embryos in nuclear cycle 14. The time constant determined from these fits is  $\tau_n = 68.9 \pm 17.6$  s (mean  $\pm$  SD). Thus, any disequilibrium in Bcd concentration between the nucleus and the surrounding cytoplasm will be corrected within roughly 1 or 2 min, which is quite fast on the scale of the nuclear cycles. In particular, this time is short enough that at each moment during interphase interval III (cf. Figure 4A), the nuclear concentration should be in steady state. Why, then, is it drifting downward by  $\sim 30\%$ ?

### Geometric Factors Correlate with Nuclear Bcd Concentration Reduction during Interphase

The sizes of nuclei during interphase are not constant; their diameters approximately double in size, as shown quantitatively in Figure 4C. Then perhaps the simplest hypothesis, which could explain the drop in intranuclear Bcd

concentration that is evident during interphase interval III, is that as the nuclei increase in volume, the intranuclear concentration is reduced by dilution. Indeed, the model above predicts that the steady state number of molecules inside the nucleus is given by  $n_{\infty} = k_{in}\tau_n C_{out}$ , and hence the concentration will be given by  $C_{in} = n_{\infty}/(4\pi r_n^3/3)$ , where  $r_n$  is the radius of the nucleus, or  $C_{in}/C_{out} = 3k_{in}\tau_n/(4\pi r_n^3)$ ; if all other parameters are fixed, the product  $C_{in}r_n^3$  should be constant. In fact this prediction is not consistent with the data:  $C_{in}r_n^3$  is an increasing function of time during interphase interval III (green curve in Figure 4D).

To understand the concentration decrease during interval III it may be useful to look more carefully at the physical factors that determine the rate of transport into the nucleus,  $k_{in}$ . The largest possible value for  $k_{in}$  can be calculated by assuming that the entire spherical surface of the nuclei is a perfect absorber for Bcd molecules that arrive via diffusion. Consideration of this limit is inspired by ligand binding to receptors on a bacterial cell surface (Berg and Purcell, 1977) and is analogous to the diffusion-limited rate constant for an enzymatic reaction (Fersht, 1985). Transport occurs through discrete nuclear pores, but the nuclei have of the order of 2500 nuclear pore complexes on their surface (Kiseleva et al., 2001) or 20–40 pores per square micron. If each pore acts as an absorber with a radius of a few nanometers, then this density of pores may be sufficient to make the entire nucleus act as an almost perfect absorber (Berg and Purcell, 1977). If this is true, the rate of Bcd transport into the nucleus should be given by the maximal, diffusion-limited rate  $k_{in} = 4\pi r_n D$ , where  $D$  is the diffusion constant of Bcd in the surrounding cytoplasm. Diffusion-limited transport means that, as the nuclei increase in size, the flux into the nucleus becomes larger, and this should partially offset the effect of dilution. More quantitatively, with  $k_{in} = 4\pi r_n D$  our simple model predicts that

$$\frac{C_{in}}{C_{out}} = \frac{3D\tau_n}{r_n^2}. \quad (4)$$

We have seen that the cytoplasmic concentration  $C_{out}$  and the recovery time  $\tau_n$  both are approximately constant during interphase, so we predict that the product  $C_{in}r_n^2$  should be constant, which is consistent with our data, as Figure 4D shows.

The combination of this result with the photobleaching experiment supports a picture in which nuclear Bcd is in rapid dynamic equilibrium with cytoplasmic Bcd and the transport into the nucleus is as fast as possible, being limited by cytoplasmic diffusion. All of the quantities in Equation 4 are directly measured except for the diffusion constant  $D$ . Thus this simple model predicts a cytoplasmic diffusion constant in terms of our other data,  $D = (C_{in}/C_{out})(r_n^2/3\tau_n)$ . The result, as shown in Figure 4D, is  $D = 0.37 \pm 0.05 \mu\text{m}^2/\text{s}$  (mean  $\pm$  SD). Although our results in Figure 4D are consistent with a simple model, there are several caveats. In particular, the nuclear pores might not act as perfect absorbers, either because

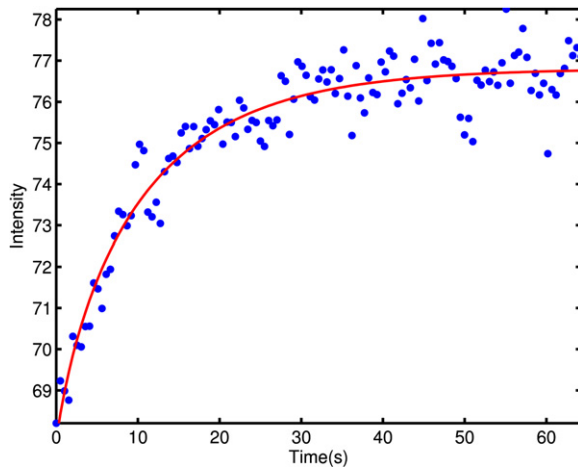


**Figure 5. Cortical Diffusion Constant Measurements by Fluorescence Recovery after Photobleaching**

Recovery curve of bleached wild-type *Drosophila* embryos expressing Bcd-GFP during mitosis 13. Bleaching was done with a scanning two-photon microscope in a volume of  $16 \times 16 \times 7 \mu\text{m}^3$  at the anterior tip of the egg. The bleaching pulse was generated by increasing the laser power 2-fold for a duration of 5 s. Data points are spaced at 0.5 s and are shown as blue dots. Red curve represents a fit to the solution of the diffusion equation (see [Experimental Procedures](#)), yielding a diffusion constant  $D = 0.27 \pm 0.07 \mu\text{m}^2/\text{s}$ .

the kinetics of transport through the pore itself are too slow (but this is unlikely; see [Kubitscheck et al., 2005](#)) or because competition among many protein species lowers the efficiency for transport of Bcd. We thus view the diffusion constant which emerges from the analysis of [Figure 4D](#) not as a measurement, but as a prediction to be tested by more direct experiments.

#### Bcd-GFP Diffusion in the Cortical Cytoplasm

To directly measure the diffusion constant of Bcd-GFP in the cortical cytoplasm, we measured the dynamics of recovery after pattern photobleaching. A rectangular volume  $16 \times 16 \times 7 \mu\text{m}^3$  in the anterior cytoplasm of Bcd-GFP-expressing embryos was photobleached during mitosis 13, when Bcd-GFP is uniformly distributed (locally) throughout the cortical cytoplasm and the cytoplasmic concentration is relatively high. A typical recovery curve is shown in [Figure 5](#). Recovery curves were fit to solutions of the diffusion equation to estimate  $D$  (see [Experimental Procedures](#)). From a total of 21 recovery curves in four embryos, our analysis provided a cytoplasmic diffusion constant  $D = 0.30 \pm 0.09 \mu\text{m}^2/\text{s}$  (mean  $\pm$  SD) during mitosis 13, which is very close to our estimate from the transport model.

This cortical diffusion constant is surprisingly small, especially given earlier measurements ([Gregor et al., 2005](#)), which showed significantly higher diffusion constants for biologically inert molecules injected into eggs. As we discuss below, it is very difficult to reconcile the small diffusion constant measured for Bcd-GFP with the fact that

the gradient forms in about one hour and remains stable over nuclear cycles 10–14. Within the SDD model, the gradient would never reach steady state with our measured small diffusion constant for Bcd-GFP, given the obvious developmental time constraints.

#### Cortex versus Core

The diffusion constants for Bcd protein we measure on the surface of the embryos would not be representative of the embryo as a whole if the cortex contains structures that trapped the protein or slowed its diffusion. The classic example of this effect is the slowing of calcium ion diffusion in neurons ([Hodgkin and Keynes, 1957](#)). In the [Supplemental Data](#), we show mathematically how the presence of binding sites would affect diffusion and observed Bcd concentration in the context of the SDD model. The result is that the presence of fixed binding sites should both slow the diffusion and enhance the total (bound + free) concentration of Bcd, both in proportion to the density of sites.

In sectioned cycle 14 embryos ([Figure 6A](#)), we do in fact see a significantly higher concentration of Bcd in the cortex relative to the central core of the egg. The intensity ratio between the cortex and the core increases in an approximately exponential fashion with progressing nuclear cycles and the increasing number of nuclei in the cortical cytoplasm (see [Figure 6D](#)). This suggests that structures which bind Bcd in the cortex are associated with the nuclei themselves. The roughly 10-fold enhancement of Bcd concentration, presumably as a result of binding to an enhanced density of fixed sites near the cortex, would be consistent with diffusion constants being an order of magnitude larger in the core of the embryo (see [Equation S9](#) in [Supplemental Data](#)), although we are unable to measure this directly.

#### Bcd Diffusion and Degradation in Unfertilized Eggs

To evaluate whether the presence of nuclei or some nuclear-related cytoplasmic structure changes the diffusive behavior of Bcd protein in the cortex, we examined the movement of Bcd in the cortex of unfertilized eggs. Although such eggs have only a single female pronucleus and do not undergo the progressive reorganization of the cortical cytoplasm associated with normal development, they still initiate translation of *bcd* RNA when the egg is laid. In contrast to the syncytial blastoderm stages described above, Bcd protein in unfertilized eggs shows no obvious enrichment in the cortex (see [Figure 6A](#)). To determine the Bcd diffusion constant in such eggs, we performed photobleaching experiments identical to those described earlier for fertilized eggs. In seven measurements on three eggs, the diffusion constant was  $D = 0.35 \pm 0.12 \mu\text{m}^2/\text{s}$ , which is nearly identical to that measured in the cortical cytoplasm of embryos. We conclude that the diffusive behavior measured in the cortex is not dependent on the presence of nuclei or associated cytoplasmic structure and may in fact represent the general behavior of all regions of the egg. In particular, to the extent that the unorganized cortex of the unfertilized egg

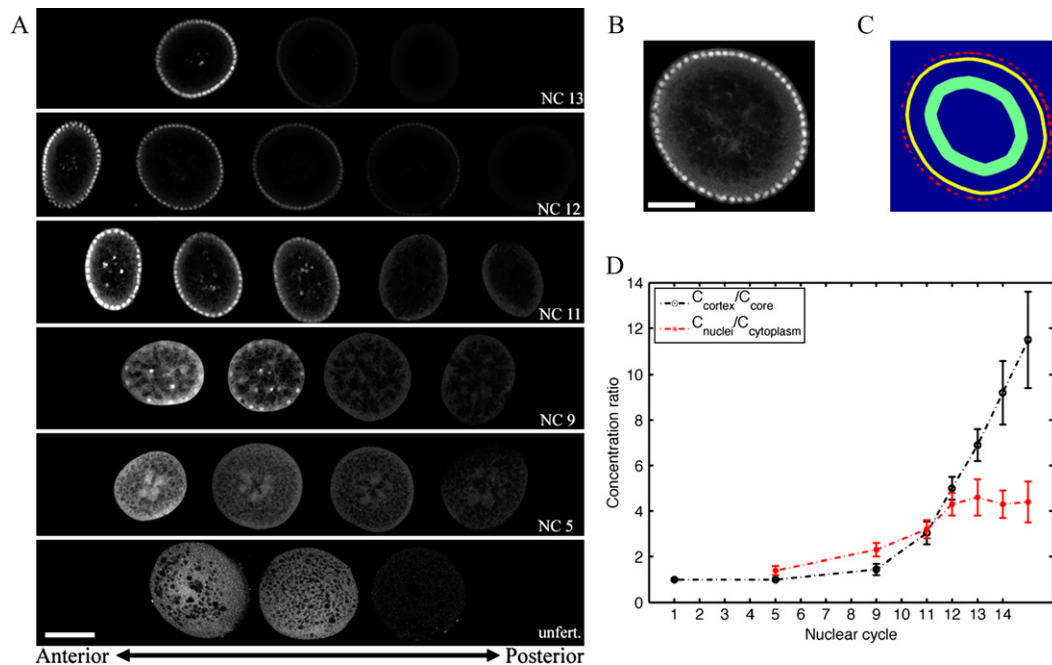


**Figure 6. Bcd Concentration Accumulation at the Egg's Cortex**

(A) Confocal images of hand-cut sections of formaldehyde-fixed wild-type *Drosophila* embryos. (Scale bar is 100  $\mu\text{m}$ .) Embryos have been stained with Bcd antibodies prior to cutting. Each row corresponds to a single embryo with sections ordered from anterior (left) to posterior (right) parts of the embryo during nuclear cycles 13, 12, 11, 9, and 5 (top to bottom). Bottom row shows a Bcd antibody staining of an unfertilized egg.

(B) Typical anterior slice of hand-cut embryo stained with Bcd antibodies (close-up of second slice from the right in second row of (A); scale bar is 50  $\mu\text{m}$ ).

(C) Mask used to extract concentration averages in (B). Red area corresponds to nuclear mask, yellow area corresponds to cytoplasmic mask, and green area corresponds to core area.

(D) Ratio of cytoplasmic Bcd concentration in the cortex and the inner core of the egg (black curve) and ratio of nuclear Bcd concentration and adjacent cytoplasmic Bcd concentration (red curve), both as a function of nuclear cycle. Concentrations are extracted from cut sections of (A; mean and SD across embryos).

approximates the environment in the central core of the fertilized egg, our results argue against the possibility that the central cytoplasm would provide a faster path for Bcd diffusion (see Discussion).

Although diffusion constants appear to be identical, the fertilized or unfertilized state of the egg may still impact the final distribution of Bcd protein. To assess this possibility, we measured the average Bcd-GFP fluorescence intensity in 400  $\mu\text{m}^2$  regions near the anterior and posterior poles and compared the results with those from similar measurements in fertilized eggs. (A more detailed comparison of full in vivo gradients in unfertilized and fertilized eggs will be presented elsewhere.) In the fertilized eggs, intensities were  $3.8 \pm 0.4$  times larger at the anterior pole than at the posterior (mean and SD over 13 embryos). This ratio is not as large as the full dynamic range of the gradient (cf. Figure 1C) because the averaging region is chosen relatively large so as to have a robust signal from the unfertilized eggs.

In the unfertilized eggs, we found that Bcd intensities at the posterior portion of unfertilized eggs are reproducibly greater than the near background levels observed in that region of fertilized eggs (data not shown), which is in

agreement with earlier findings by Driever and Nüsslein-Volhard (1988a). At the anterior pole, intensities were lower and the overall ratio was  $1.5 \pm 0.3$  (mean and SD over 13 embryos). At 5 hr, when the anterior intensity of Bcd-GFP in unfertilized eggs was more nearly equal to that in fertilized eggs at cycle 14, the anterior/posterior ratio had not changed ( $1.3 \pm 0.3$ ;  $n = 13$  embryos).

These observations suggest that gradient formation in unfertilized eggs differs from that of fertilized eggs in two significant respects: The levels achieved at the posterior pole are higher, and the overall shape is flatter. Since the level of Bcd at the posterior pole would be expected to be greatly influenced by degradation, this provides support for considering models in which the nuclei present in fertilized eggs contribute to the degradation process itself (see Discussion).

## DISCUSSION

Our principal results, together with those of previous work (Driever and Nüsslein-Volhard, 1988a, 1988b; Houchmandzadeh et al., 2002; Gregor et al., 2005), provide the

following foundation for any mechanistic model for the formation or read out of the Bcd gradient:

1. The gradient is approximately (but not necessarily exactly) an exponential decay in intranuclear (and cytoplasmic) concentration that is established rapidly (less than 90 min).
2. Bcd diffuses relatively slowly ( $D = 0.3 \mu\text{m}^2/\text{s}$ ) in the cortical cytoplasm containing the nuclei.
3. The Bcd gradient is stable over nuclear cycles 10–14, when the number of nuclei is growing by a factor of two with each division and Bcd is concentrated and released from nuclei in a dynamic process. In particular, the initial postinterphase concentration in nuclei in successive cycles is constant to at least 10% but decays by approximately 30% during the subsequent interphase period.
4. Bcd is not simply trapped in nuclei; rather, it is in dynamic equilibrium between influx and efflux with the cytoplasm and, possibly, intranuclear degradation.
5. The total (bound + free) concentration of Bcd in the cortical cytoplasm is distinctly higher than in the yolk.
6. The spatial shape of the Bcd gradient (the length constant for an exponential decay) scales with embryo length over a factor of five range in lengths in different dipteran species (Gregor et al., 2005).

### Problems with the Simplest Gradient Model

The most widely considered and simplest model for Bcd gradient formation—namely the SDD model—consists of a source of protein synthesis localized at the anterior pole, intracellular Bcd diffusion away from the source, and spatially uniform degradation by a first-order reaction. If Bcd molecules diffuse throughout the embryo with diffusion constant  $D$  and are degraded with lifetime  $\tau$ , the concentration of Bcd protein in this simple model obeys

$$\frac{\partial C_{\text{Bcd}}(\vec{r}, t)}{\partial t} = D \nabla^2 C_{\text{Bcd}}(\vec{r}, t) - \frac{1}{\tau} C_{\text{Bcd}}(\vec{r}, t). \quad (5)$$

The source is described as a boundary condition at the anterior pole ( $x = 0$ ).

This model predicts the steady state concentration profile, and its principal virtue is that it produces the experimentally observed exponential decay,  $C(x) = C(0)\exp(-x/\lambda)$ , with  $\lambda = \sqrt{D\tau}$ . Steady state is reached, however, only after a time much greater than the protein lifetime  $\tau$ , assuming (as observed) that the length constant  $\lambda$  is much smaller than the length of the embryo. Since we have no direct measurement of  $\tau$ , it is more useful to say that the time required to reach steady state is  $\tau_{\text{ss}} \gg \lambda^2/D$ . The observed concentration profiles have  $\lambda \sim 100 \mu\text{m}$ , which means that to reach a steady state within 90 min requires that the diffusion constant of Bcd must be  $D \gg 2 \mu\text{m}^2/\text{s}$ . This is an order of magnitude larger than what we measure directly in photobleaching experiments (Figure 5) or what we infer indirectly from the dynamics of nuclear-cytoplasmic exchange (Figure 4D).

It could have been that the diffusion constants were slow but that correspondingly the gradient did not reach steady state during the blastodermal stages of development. Alternatively, the apparent steady state behavior of the gradient for cycles 10 through 14 would not be surprising if diffusion constants were large. The paradox is that we observe *both* slow diffusion and the rapid establishment of a steady state. Simply put, the diffusion processes that we observe cannot be the ones which generate the steady state profile because they are too slow.

There are, broadly speaking, three possible ways in which the paradox of slow diffusion and rapid arrival at the steady state could be resolved: Diffusion in the bulk of the embryo could be faster than we observe in the cortex, diffusion could be faster in the first hour after fertilization (where we were unable to measure Bcd), or the effective diffusion constants could be different on different time scales ( $\sim 1$  min versus  $\sim 1$  hr) because of active transport mechanisms. These possibilities are discussed in the [Supplemental Data](#).

### Nuclear Degradation and Scaling of the Bcd Gradient

Perhaps the most striking result in the present work is the dynamic exchange of Bcd from cytoplasm to nuclei. In cycle 14, the number of nuclei, the enhancement of cytoplasmic concentration near the cortex, and the further enhancement of concentration above this in the nuclei all combine to mean that  $\sim 40\%$  of the Bcd molecules in the entire embryo are localized in the nuclei (see [Experimental Procedures](#) for details). Thus, rather than passively sampling a large excess of molecules in the cytoplasm, the nuclei *must* perturb the gradient significantly. In particular, it is natural to ask if events inside the nucleus could influence or even dominate Bcd degradation (Dhananjayan et al., 2005; Collins and Tansey, 2006). Although our results do not directly prove this assertion, it is intriguing that there is a smaller anterior-to-posterior ratio of Bcd concentration in unfertilized eggs than in fertilized eggs undergoing nuclear divisions. Driever and Nüsslein-Volhard (1988a) also noted a pronounced increase in Bcd concentration in unfertilized eggs after the first hour, which is consistent with our observations (data not shown).

What is particularly interesting about the possibility of nuclear involvement in degradation is that it can naturally solve the scaling problem. To illustrate how this can work, it is useful to consider an extreme (and admittedly unrealistic) model. Suppose that there is no degradation of Bicoid in the bulk of the embryo, but the degradation rate inside nuclei is so high that once molecules diffuse into the cortical layer of nuclei they never escape. Then rather than a model in which degradation is a specific term in the dynamics of the Bcd concentration, as in Equation 5, one can think of the degradation process as a boundary condition near the embryo surface. In this limit, no lifetimes or rate constants appear in the equations, and so the steady state is determined by balancing boundary conditions—a source at the anterior pole and a distributed

“sink” along the cortical surface. As a result, the steady state profile depends only on the geometry of the embryo itself and hence automatically scales as one considers embryos of different sizes.

As a more realistic model, imagine a two-dimensional array of nuclei at positions near the embryo surface, and let us assume that degradation of protein within the nuclei occurs with lifetime  $\tau_{\text{nuc}}$ , in contrast to the lifetime  $\tau$  in the cytoplasm outside the nuclei. If  $\tau \gg \tau_{\text{nuc}}$ , then almost all the degradation will happen in the nuclei, and the effective rate of degradation, averaged over some reasonable volume, can be shown to be proportional to the density of nuclei in that volume,  $\tau_{\text{eff}} \propto 1/\rho_{\text{nuc}}$ , so that the length constant  $\lambda = \sqrt{D\tau} \propto 1/\sqrt{\rho_{\text{nuc}}}$ . Importantly, the number of nuclei at a given cycle is constant across embryos of very different size (Gregor et al., 2005) so that  $\rho_{\text{nuc}} = N_{\text{nuc}}/(A\ell)$ , where  $A$  is the surface area of the egg and  $\ell$  is the thickness of the cortical layer ( $\ell \sim 30 \mu\text{m}$  in cycle 14). Different size embryos from different flies seem to have similar aspect ratios, so we expect  $A \sim GL^2$ , where  $G \sim 0.3$  reflects this geometry. The result is that  $\rho_{\text{nuc}} = N_{\text{nuc}}/GL^2\ell$  so that  $\lambda \propto 1/\sqrt{\rho_{\text{nuc}}}$  is equivalent to  $\lambda \propto L$ . Thus, if trapping of Bcd in the nuclei dominates the dynamics and if nuclei are ordered in space and time as observed, then we have scaling automatically. Within this model, scaling is achieved because the number of nuclei is conserved in differently sized eggs, and hence the nuclear density is reduced in larger eggs.

One central problem of models in which the nuclei play an essential role is that the number of nuclei is changing, doubling every 9 to 12 min during the crucial period of development. There is no evidence that the Bcd profile changes shape during this time. In the simplest view, if nuclear processes dominate the degradation of Bcd, then the effective lifetime should change by a factor of two with each successive cycle, thus changing the length constant  $\lambda$  by a factor of four from cycle 10 to 14. But this simple view breaks down if the other relevant parameters are changing. Over the course of these four doublings in the number of nuclei, the radius of the nuclei changes by nearly a factor of two (Figure 4C), and the thickness  $\ell$  of the cortical layer changes by a factor of three (Foe et al., 1993). In addition, the partitioning of Bcd molecules between the cortical layer and the interior bulk of the egg changes substantially (Figure 6D). In a coarse-grained picture, if degradation is dominated by events inside the nuclei, then the effective lifetime of a Bcd molecule in the embryo should depend on the fraction of molecules localized in nuclei; the different factors listed above in fact conspire so that this fraction remains constant across cycles 11 through 14, within the  $\sim 20\%$  accuracy of our estimates (see Experimental Procedures).

### Perspective

Our earlier work (Gregor et al., 2005) established that molecular motion in the embryo is described well by the diffusion equation on the time ( $\sim 1$  hr) and space ( $\sim 0.1$  mm) scales of relevance for morphogenesis. The present work shows that diffusion is an equally good description

of Bicoid transport on the scale of minutes and microns. The difficulty is that the relevant diffusion constants differ by more than an order of magnitude. To explain our observation that the Bcd gradient reaches a nuclear steady state very quickly we need the larger diffusion constants, but the dynamics of transport into and out of the nuclei are consistent with the smaller diffusion constant, which we also measure directly. We have discussed possible resolutions of this paradox, but new experiments will be required to decide which of these is correct.

The most dramatic qualitative feature that we see in watching the development of the embryos expressing Bcd-GFP is the filling and emptying of the nuclei. Quantitatively, this results in a startling juxtaposition of dynamics and stability. Thus, although Bcd concentrations vary in time over a factor of four during the course of a mitotic cycle, the nuclear concentration near the start of interphase is reproducible with  $\sim 10\%$  accuracy from cycle to cycle. Although the number of nuclei is changing by a factor of 16 from cycle 10 to cycle 14, the total number of Bcd molecules that are localized in nuclei changes hardly at all. At our present level of understanding, both these examples of stability in the presence of change seem to be the result of cancellation among several independent processes, which is implausible. One way of summarizing the problem is that the simplest model looks like it works, but this is only because many parameters have been adjusted to make it work, leaving the simplest model as an effective description of the dynamics after the mechanisms responsible for this adjustment have done their job. This layer of mechanisms remains to be discovered.

## EXPERIMENTAL PROCEDURES

### Construction of P[*egfp-bcd*]

P[*egfp-bcd*] transcription is driven by known *bcd* enhancers upstream of the 5' UTR and in the first intron. This transcript contains *bcd*'s natural 5' and 3' UTRs which are known to mediate the localization and translation of normal *bcd* mRNA. Thus by using the endogenous regulates of *bcd* transcription and translation, our construct was designed to be maternally expressed and localized to the anterior pole.

pNBGA1 containing a 6.5 kb *D. melanogaster* genomic fragment of the entire *bcd* gene, with the GFP coding region inserted directly upstream of and in frame with the first exon of *bcd*, was kindly provided by Tulle Hazelrigg (Hazelrigg et al., 1998). This plasmid was digested with NheI and SphI to remove GFP and replace it with either eGFP generated by PCR from pStinger (Barolo et al., 2000) using primers appended with NheI and SphI restriction sites. The resulting fusion gene was subsequently subcloned into the BamHI and EcoRI sites of pCaSpeR4 (Thummel and Pirrotta, 1992) to generate P[*egfp-bcd*].

### Fly Transformation

We followed standard *P* element transformation procedures (Spradling and Rubin, 1982). We injected 0.4 mg/ml of construct DNA together with 0.1 mg/ml helper plasmid pTURBO, which expresses the transposase into *D. melanogaster yw* embryos. We scored several different P[*egfp-bcd*] insertions, including insertions on chromosomes I, II, and X. Stocks were established for each of these.

### Fly Stocks and Genetics

For all experiments with flies expressing *egfp-bcd* we used a stock with an X-chromosomal insertion of P[*egfp-bcd*]. For substitution of

endogenous *bcd* we conducted the mutant crosses of *egfp-bcd* with *bcd<sup>E1</sup>*, *p<sup>P</sup>/TM3*, *Sb* to generate *egfp-bcd;bcd<sup>E1</sup>*, *p<sup>P</sup>*. Unfertilized eggs of Oregon R wild-type *D. melanogaster* flies and of *bcd<sup>E1</sup>;egfp-bcd* flies were produced using sterile males generated from *C(1,Y),yB/0*.

### Immunostaining of Embryos

All *D. melanogaster* embryos were collected at 25°C. Embryos expressing Bcd-GFP were formaldehyde fixed (for 20 min in 3.7% formaldehyde/PBS:heptane and devitellinized in heptane:methanol), all other embryos were heat fixed, and the eggs were subsequently labeled with fluorescent probes following previously published protocols (Wieschaus and Nüsslein-Volhard, 1986). We used rat anti-Bcd and rabbit anti-HB antibodies, gifts of J. Reinitz (Kossmann et al., 1998), as well as guinea pig anti-GFP (Molecular Probes) and rabbit anti-GFP (Chemicon). Secondary antibodies were conjugated with Alexa-488, Alexa-546, and Cy5-647 (Molecular Probes). Nuclei were labeled with DNA probes YOYO1 or TOTO3 (Molecular Probes). Eggs were mounted in AquaPolymount (Polysciences, Inc.).

### Cut-Sections of Fixed Eggs

Heat-fixed embryos were embedded in 50% glycerol and hand-cut with a sharp razor blade. The embryos employed were stained with Bcd antibodies (see above), and the cut-sections were imaged focusing at the top-most surface of the section. To exclude a misrepresentation of our experiment due to problems with permeabilization and antibody penetration into the embryo, we tested and quantified two versions of this experiment: in the first version we heat-fixed embryos stained with Bcd antibodies and hand-cut the eggs after the staining procedure was completed; in the second version of the experiment we heat-fixed the embryos and hand-cut them before running the staining procedure. Both procedures led to the same quantitative results.

### Imaging of Fixed Tissue by Confocal Microscopy

High-resolution digital images (1024 × 1024, 12 bits per pixel) of fixed eggs were obtained on a Zeiss LSM 510 confocal microscope with a Zeiss 20× (NA 0.45) A-plan objective. Images were focused at mid-embryo to avoid geometric distortion for gradient extraction experiments. For measurements of nuclear fluorescence intensities eggs were flattened with a cover slip to maximize the number of nuclei at the focal top surface.

### Live Imaging by Two-Photon Microscopy

Living embryos were collected 0–15 min after egg deposition, dechorionated, glued onto a cover slip, and immersed in halocarbon oil (Sigma-Aldrich) or *dH<sub>2</sub>O*. Two-photon microscopy (Denk et al., 1990) was performed using a custom-built scanning microscope similar in design to that of reference (Svoboda et al., 1997). Time-lapse image sequences were taken with a Zeiss Plan-Neofluar multi-immersion objective (25×, NA 0.8) and an excitation wavelength of 900–920 nm, minimizing embryonic yolk autofluorescence. Average laser power at the specimen was between 10 and 30 mW.

### Photobleaching Experiments

Bcd-GFP-expressing embryos were mounted as described above. Photobleaching of individual nuclei was performed using our scanning two-photon microscope by reducing the scan-field 8-fold while keeping the laser power constant, effectively increasing the power per pixel 64-fold for a duration of 5 s. Subsequently the recovery curve was recorded in 0.5 s time bins with the original scan-field, where the recording power has been adjusted to avoid further photobleaching. The bleach-volume ( $16 \times 16 \times 7 \mu\text{m}^3$ ) generated with the 25× (NA 0.8) Zeiss Plan-Neofluar multi-immersion objective was measured separately using fluorescently-labeled 40 kDa-dextran *dH<sub>2</sub>O* solution diluted in polyethylene. Cytoplasmic photobleaching was performed by rapid modulation of the beam with a KDP\* Pockels Cell (model 350-50; Conoptics, Danbury, CT) to generate the bleaching and monitoring

intensities (Axelrod et al., 1976). In these experiments the power modulation at the specimen was 2-fold, the bleach pulse was 6 s, and the bleach-volume was  $16 \times 16 \times 7 \mu\text{m}^3$ . Data was fitted to the exact solution of the 3D diffusion equation (Brown et al., 1999).

### Profile Quantification

Bcd protein profiles were extracted from images of stained embryos using software routines (MATLAB, MathWorks, Natick, MA) that allowed a circular window of the size of a nucleus to be systematically moved along the outer edge of the embryo (Houchmandzadeh et al., 2002). At each position, the average pixel intensity within the window was plotted versus the projection of the window center along the AP-axis of the embryo. Measurements of the Bcd concentration were made separately along the dorsal and ventral sides of the embryo. All embryos were prepared, and images were taken under the same conditions: (i) all embryos were formaldehyde fixed for 20 min, (ii) embryos were stained and washed together in the same tube, and (iii) all images were taken with the same microscope settings in a single acquisition cycle.

### Comparing Gradients of Antibody Staining and GFP Fluorescence

Gradients of double stained embryos expressing Bcd-GFP were compared in a scatter plot with the different gradient visualization methods (antibody against Bcd, antibody against GFP and endogenous GFP fluorescence) on each axis. Scatter plots of gradients of identical shape should only have data points on the diagonal. We tested this method for comparing intensity profiles using artificially generated distributions of gradients with different mean shapes, and we obtained significant power-law dependencies for distributions that differed by more than 4% of their mean (the mean is characterized by the average length constant of artificially-generated, exponentially decaying intensity profiles).

### Fraction of Bcd Molecules in Nuclei

To estimate the relative number of Bcd molecules in nuclei, cortical cytoplasm and the core of an embryo of length  $L \sim 490 \mu\text{m}$ , we consider a cross-sectional slice of thickness  $\Delta x$  with volume  $V_{\text{tot}} = \pi R^2 \Delta x$ , where  $R \sim 90 \mu\text{m}$  is the radius of the slice (see Figure 2A). The number of nuclei in the slice is given by  $(N/L)\Delta x$ , where  $N$  is the total number of nuclei in the embryo, typically  $\sim 6000$  during nuclear cycle 14; hence the total nuclear volume is  $V_{\text{nuc}} = \frac{4}{3}\pi r_n^3 N \frac{\Delta x}{L}$ , with nuclear radius  $r_n$  (see Figure 1C for values). The core volume is given by  $V_{\text{core}} = \pi(R - \ell)^2 \Delta x$ , with  $\ell$  being the thickness of the cortical cytoplasm. The relative number of Bcd molecules in nuclei, cortical cytoplasm, and the core of an embryo are then respectively given by  $n_{\text{core}} = C_{\text{core}} V_{\text{core}}$ ,  $n_{\text{nuc}} = C_{\text{nuc}} V_{\text{nuc}}$  and  $n_{\text{cort.-cyt.}} = C_{\text{cort.-cyt.}} (V_{\text{tot}} - V_{\text{core}} - V_{\text{nuc}})$ , with core, nuclear, and cortical Bcd concentrations  $C_{\text{core}}$ ,  $C_{\text{nuc}}$  and  $C_{\text{cort.-cyt.}}$ , respectively. Finally, the fraction of Bcd molecules in the nuclei is given by

$$f_{\text{nuc}} = \frac{n_{\text{nuc}}}{n_{\text{core}} + n_{\text{nuc}} + n_{\text{cort.-cyt.}}} \quad (6)$$

To estimate  $f_{\text{nuc}}$  for nuclear cycles 11 to 14, we use cortical thicknesses  $\ell$  of 11  $\mu\text{m}$ , 15  $\mu\text{m}$ , 24  $\mu\text{m}$ , and 31  $\mu\text{m}$ , respectively (Foe et al., 1993). Reading the respective concentrations and nuclear radii from our data (see Figures 2D and 1C), we obtain the fraction of nuclear Bcd molecules in the nucleus: 33%, 39%, 41%, and 41% for nuclear cycles 11 to 14, respectively. Our estimated accuracy on these values is  $\sim 20\%$ .

### Supplemental Data

Supplemental Data include an extended Figure 2 legend, Discussion, References, and one movie and can be found with this article online at <http://www.cell.com/cgi/content/full/130/1/141/DC1/>.

## ACKNOWLEDGMENTS

We thank N. Bisaria, M. Coppey, J. Drocco, T. Hazelrigg, J. Kinney, R. Samantha, and G. Tkacik. This work was supported in part by the Howard Hughes Medical Institute, the MRSEC Program of the National Science Foundation under Award Number DMR-0213706, and by NIH grants P50 GM071508 and R01 GM077599.

Received: October 15, 2006

Revised: February 15, 2007

Accepted: May 3, 2007

Published: July 12, 2007

## REFERENCES

- Ariizumi, T., and Asashima, M. (1995). Control of the embryonic body plan by activin during amphibian development. *Zoolog. Sci.* *12*, 509–521.
- Axelrod, D., Koppel, D.E., Schlessinger, J., Elson, E., and Webb, W.W. (1976). Mobility measurement by analysis of fluorescence photobleaching recovery kinetics. *Biophys. J.* *16*, 1055–1069.
- Barolo, S., Carver, L.A., and Posakony, J.W. (2000). GFP and beta-galactosidase transformation vectors for promoter/enhancer analysis in *Drosophila*. *Biotechniques* *29*, 726–732.
- Berg, H.C., and Purcell, E.M. (1977). Physics of chemoreception. *Biophys. J.* *20*, 193–219.
- Brown, E.B., Wu, E.S., Zipfel, W., and Webb, W.W. (1999). Measurement of molecular diffusion in solution by multiphoton fluorescence photobleaching recovery. *Biophys. J.* *77*, 2837–2849.
- Collins, G.A., and Tansey, W.P. (2006). The proteasome: a utility tool for transcription? *Curr. Opin. Genet. Dev.* *16*, 197–202.
- Crick, F. (1970). Diffusion in embryogenesis. *Nature* *225*, 420–422.
- Denk, W., Strickler, J.H., and Webb, W.W. (1990). Two-photon laser scanning fluorescence microscopy. *Science* *248*, 73–76.
- Dhananjayan, S.C., Ismail, A., and Nawaz, Z. (2005). Ubiquitin and control of transcription. *Essays Biochem.* *41*, 69–80.
- Driever, W., and Nüsslein-Volhard, C. (1988a). A gradient of Bicoid protein in *Drosophila* embryos. *Cell* *54*, 83–93.
- Driever, W., and Nüsslein-Volhard, C. (1988b). The Bicoid protein determines position in the *Drosophila* embryo. *Cell* *54*, 95–104.
- Ephrussi, A., and St Johnston, D. (2004). Seeing Is Believing: The Bicoid Morphogen Gradient Matures. *Cell* *116*, 143–152.
- Fersht, A. (1985). *Enzyme Structure and Mechanism* (San Francisco, CA: Freeman).
- Foe, V.E., Odell, G.M., and Edgar, B.A. (1993). Mitosis and morphogenesis in the *Drosophila* embryo: point and counterpoint. In *The Development of Drosophila*, M. Bate and A. Martinez-Arias, eds. (Plainview, NY: Cold Spring Harbor Laboratory Press), pp. 149–300.
- Gregor, T., Bialek, W., de Ruyter van Steveninck, R.R., Tank, D.W., and Wieschaus, E.F. (2005). Diffusion and scaling during early embryonic pattern formation. *Proc. Natl. Acad. Sci. USA* *102*, 18403–18407.
- Hazelrigg, T., Liu, N., Hong, Y., and Wang, S. (1998). GFP expression in *Drosophila* tissues: time requirements for formation of a fluorescent product. *Dev. Biol.* *199*, 245–249.
- Hodgkin, A.L., and Keynes, R.D. (1957). Movements of labelled calcium in giant axons. *J. Physiol.* *138*, 253–281.
- Houchmandzadeh, B., Wieschaus, E., and Leibler, S. (2002). Establishment of developmental precision and proportions in the early *Drosophila* embryo. *Nature* *415*, 798–802.
- Kiseleva, E., Rutherford, S., Cotter, L.M., Allen, T.D., and Goldberg, M.W. (2001). Steps of nuclear pore complex disassembly and reassembly during mitosis in early *Drosophila* embryos. *J. Cell Sci.* *114*, 3607–3618.
- Kossmann, D., Small, S., and Reinitz, J. (1998). Rapid preparation of a panel of polyclonal antibodies to *Drosophila* segmentation proteins. *Dev. Genes Evol.* *208*, 290–298.
- Kubitscheck, U., Grunwald, D., Hoekstra, A., Rohleder, D., Kues, T., Siebrasse, J.P., and Peters, R. (2005). Nuclear transport of single molecules: dwell times at the nuclear pore complex. *J. Cell Biol.* *168*, 233–243.
- Lacalli, T.C., and Harrison, L.G. (1991). From gradient to segments: models for pattern formation in early *Drosophila*. *Semin. Dev. Biol.* *2*, 107–117.
- Lawrence, P.A. (1992). *The Making of a Fly: The Genetics of Animal Design* (Oxford, UK: Blackwell Scientific).
- Spradling, A.C., and Rubin, G.M. (1982). Transposition of cloned P-elements into *Drosophila* germ line chromosomes. *Science* *218*, 341–347.
- Struhl, G., Struhl, K., and Macdonald, P.M. (1989). The gradient morphogen Bicoid is a concentration-dependent transcriptional activator. *Cell* *57*, 1259–1273.
- Svoboda, K., Denk, W., Kleinfeld, D., and Tank, D.W. (1997). *In vivo* dendritic calcium dynamics in neocortical pyramidal neurons. *Nature* *385*, 161–165.
- Thummel, C.S., and Pirrotta, V. (1992). New pCaSpeR P element vectors. *Drosoph. Inf. Serv.* *71*, 150.
- Tsien, R.Y. (1998). The green fluorescent protein. *Annu. Rev. Biochem.* *67*, 509–544.
- Wieschaus, E., and Nüsslein-Volhard, C. (1986). Looking at embryos. In *Drosophila, a Practical Approach*, D.B. Roberts, ed. (Oxford, UK: IRL Press), pp. 199–227.
- Wolpert, L. (1969). Positional information and the spatial pattern of cellular differentiation. *J. Theor. Biol.* *25*, 1–47.
- Zecca, M., Basler, K., and Struhl, G. (1995). Sequential organizing activities of engrailed, hedgehog and decapentaplegic in the *Drosophila* wing. *Development* *121*, 2265–2278.